Supplementary Electronic Materials for

Graphene Oxide Fibers by Microfluidics Assembly: A Strategy for Structural and Dimensional Control

Jaqueline F. Rocha[a,b], Leandro Hostert[a], Martha Lucia M. Bejarano[b], Roberta M. Cardoso[b], Matheus D. Santos[a], Camila M. Maroneze[a] and Mario R.Gongora-Rubio[b] and Cecilia de Carvalho Castro Silva [a,*]

[a]MackGraphe - Graphene and Nanomaterials Research Center, Mackenzie Presbyterian University, 01302-907, São Paulo, Brazil.

[b]Micromanufacturing Laboratory - Bionanomanufacturing Center - Institute for Technological Research (IPT), 05508-901, São Paulo, Brazil.

* Corresponding author: Tel: +55 -11 -27667380. E-mail: cecilia.silva@mackenzie.br (C.C.C.Silva)

This document file includes:

Supplementary Text

Figs. S1 to S12

References (1-11)

Fabrication of the 3D Flow-Focusing Microfluidic Device

The 3D flow-focusing microfluidic device was fabricated based on the low temperature co-fired ceramics (LTCC) technology that was previously reported by the research group of Gongora-Rubio[1] and which is briefly described by the following steps: The 3D device was designed to fragment the three-dimensional structure into two-dimensional sections, using AutoCAD® software (AutoDesk, Inc, USA). Each section was transferred to green ceramics tapes (951P2 and 951PX, DuPont) by UV laser cutting (355 nm wavelength) using LPKF Protolaser® U3 (LPKF Laser & Electronics AG, Garbsen, Germany). The equipment was able to fully cut the 165 and 254 µm green ceramic tapes with high resolution and following the layout of the device. The cut green ceramic sheets were aligned to reconstruct the original tri-dimensional structure, and laminated by uniaxial thermo-compression (11,8 MPa, 70ºC) for 20 minutes. The resulting material is formed by adhered tapes and it is ready for the sintering step. The ceramic stack was submitted to a two-step heating program, whereas the heating rate was fixed in 5°C·min^{-1} and two temperatures programs of 450 and 850ºC, respectively, were sustained for one hour each. After mild cooling, the ceramic block was already sintered and characterized by planned channel dimensions and predicted thickness. The device was ready for experimental studies by incorporation of needles with internal diameters of 330 µm (inlet needle) and 840 µm (outlet needle) (Nordson Corporation), and Fortron® PPS connections, using epoxy adhesives.

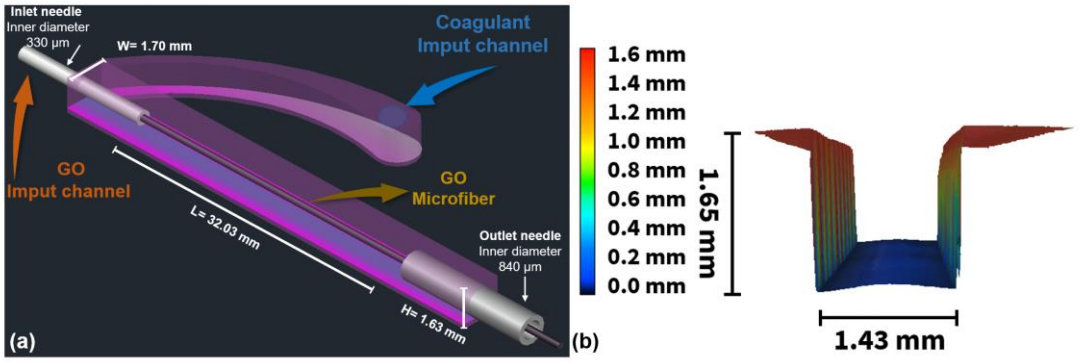

Fig. S1. 3D flow-focusing microfluidic device. (a) Schematic representation of the inside view of the microfluidic device, showing the dimensions of the channels and needles used and the formation of the GO fiber (b) 3D laser scanning microscopy image of the main channel of the final microfluidic device showing the real dimensions.

Preparation of Graphene Oxide Dispersion

For the preparation of the aqueous GO dispersion, the following steps were carried. In a flask, approximately 0.5 g of graphite (Sigma-Aldrich, 98.4% of the flakes with a particle size of 100 mm) were dispersed in 16.9 mL of concentrated sulfuric acid (Synth, 98.0% purity), leaving under stirring for 30 minutes in an ice batch. Then 0.38 g of sodium nitrate (Merck, 99.9% purity) was added. After more than 5 minutes of magnetic stirring, small portions of potassium permanganate (Synth, 99.0% purity) were added to completed 2.25 g, over a period of 1 hour, under stirring and low temperature (ice batch). After this step, the reaction was in rest for three days. Subsequently, 50 mL of sulfuric acid aqueous, 0.06 mol L^{-1}, was added slowly for 1 hour and kept under stirring for another 2 hours. Forthwith, it was then added slowly 1.5 mL of 30% (w/v) hydrogen peroxide (Sigma-Aldrich) and the mixture was stirred for another 2 hours. To finish the process, the prepared GO dispersion has been washed three times with aqueous 10% hydrochloric acid aqueous solution (Synth, 37% purity). The GO dispersion was purified using dialysis bags (porosity of 12 kDa) in distilled water, followed by the use of a fluidic diffusion cell[2], coupled to a nitrocellulose membrane (pore size of 0.22 µm) until the residual GO water reaches a pH of 5.5. The fluidic diffusion cell system allows the selection of the GO flakes with larger lateral size and avoids the damage of the GO sheets by the conventional purification process such as centrifugation[2]. Finally, the GO dispersion was concentrated to 10 mg mL^{-1} using a rotary evaporator-microprocessor (Q344M QUIMIS).

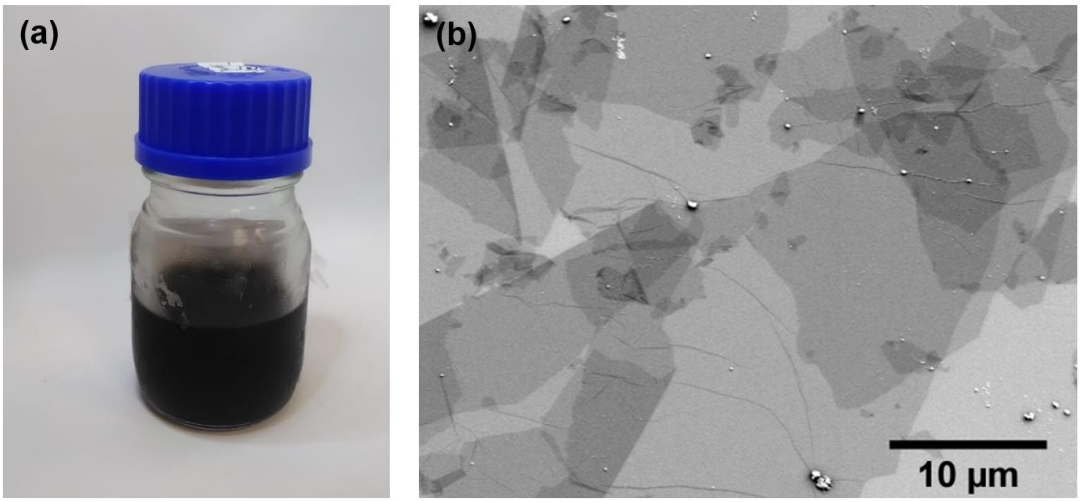

Fig. S2. GO dispersion. (a) Photograph of the synthesized GO dispersion with a concentration of 10 mg mL^{-1} and (b) Typical SEM image of the synthesized GO sheets on Si /SiO_2 substrate.

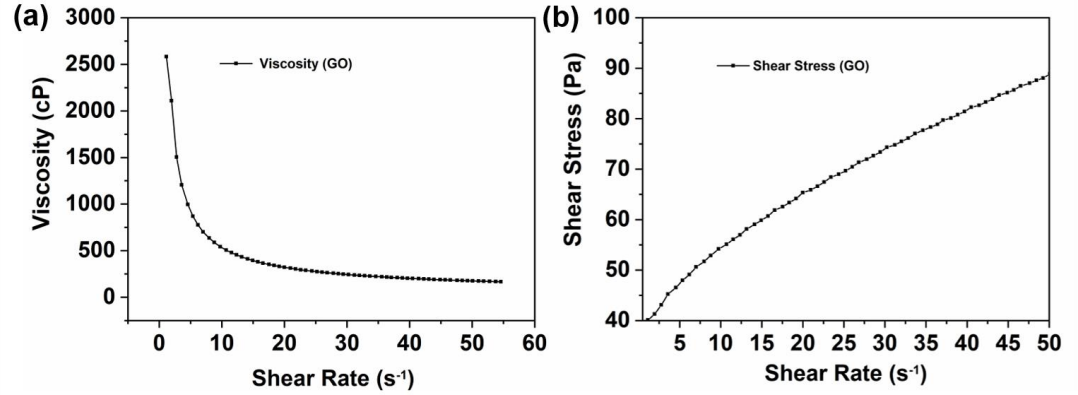

Fig. S3. Rheological behavior of the aqueous dispersions of GO (5mg mL^{-1}). (a) Viscosity and (b) Shear stress, as a function of the shear rate.

Computational Fluid Dynamics (CFD) Simulation

The flow structure in the microfluidic device was studied with the commercial CFD code ANSYS Fluent 2019 R2[3], which solves the continuity and Navier–Stokes equations through the finite volume method. The computational domain was adjusted with Design Modeler. To conduct the numerical analysis, grid systems were generated using Meshing code. Meshes with the number of cells between 5.2 x 10^5 and 1.3 x 10^7 were used to carry out the calculations.

The flow regime of the 3D flow-focusing microfluidic device developed in this work was included in the laminar regime (Re ≅ 10^{-2}). Eulerian model involved in multiphase models of ANSYS-Fluent was used to obtain velocity profiles and to observe the behavior of the fluids. This model allows for the modeling of multiple separate yet interacting phases. It is appropriate for flows in which the phases are concentrated just in portions of the domain and the volume fractions of the dispersed phase exceed 10%. To evaluate the interaction between the phases, the interphase Exchange Coefficient was calculated. For the drag coefficient, the Schiller-Naumann was considered. In the simulation, Eulerian model solves a set of momentum and continuity equations for each phase. Coupling is achieved through the pressure and interphase exchange coefficients. The way this coupling is handled depends upon the type of phases involved[3].

The phasic volume fraction α_q is calculated from a continuity equation S1 and S2:

$$\frac{1}{\rho_{rq}}\left(\frac{\partial}{\partial t}\left(\alpha_q \rho_q\right) + \nabla \cdot \left(\alpha_q \rho_q \overrightarrow{v_q}\right) = \sum_{p=1}^{n}\left(\dot{m}_{pq} - \dot{m}_{qp}\right)\right)$$

and

$$\sum_{q=1}^{n} \alpha_q = 1$$

where ρ_{rq} is the phase reference density, or the volume averaged density of the phase in the solution domain, $\overrightarrow{v_q}$ is the velocity of phase q and $\dot{m}_{pq}$ characterizes the mass transfer from the p^{th} to q^{th} phase, and $\dot{m}_{qp}$ characterizes the mass transfer from phase q to phase p, and it is possible to specify these mechanisms separately.

The CTAB and GO aqueous solutions were defined as the continuous and disperse phases, respectively. A Newtonian flow for the CTAB solution was observed. On the other hand, the GO dispersion showed a Non-Newtonian behavior described by a power-law viscosity model, $\eta = k\gamma^{n-1}$, with decreasing viscosity (η) and power-law index, $n < 1$. From the curve of viscosity in the function of shear rate, Fig. S3, an adjusted model ($R^2 = 0.9971$) with $k = 2.9254$ and $n = 0.274$ was obtained and it was used to calculate the viscosity value for GO dispersion in the computational tests. The dynamics of the velocity field v of the incompressible non-Newtonian fluid are described by the Navier–Stokes equation with the shear rate-dependent viscosity.

To solve the model equations, the following boundary conditions were considered: viscous, isothermal, incompressible and laminar flow. Aqueous CTAB solution was introduced at the side inlet and the GO solution enters at the inlet needle. Constant velocity magnitude (velocity inlet) was specified at the inlets, while zero static pressure was assigned at the outlet (pressure outlet). No-slip condition was employed at the walls. The physical properties of CTAB solution and GO dispersion were experimentally determined by rheological and density assays and are presented in Table S1.

Table S1. Physical properties of CTAB aqueous solution (0.5 mg mL^{-1}) and GO dispersion (5 mg mL^{-1}) phases used in the CFD simulations

Phase	**Density (ρ) (kg m^{-3})**	**Dynamic viscosity (μ) (kg m^{-1} s^{-1})**
CTAB	980.6	0.00129
GO	995.8	Non-Newtonian power-law viscosity model

Equations were discretized with an abounding second-order differencing scheme, i.e., upwind scheme with second-order correction, which minimized numerical diffusion in the results. The convergence of the simulations was defined by the normalized residual (root mean square error) of 1.0×10^{-5}. Streamlines colored by velocity magnitude were used to evaluate the dynamic behavior of fluids in the microfluidic device.

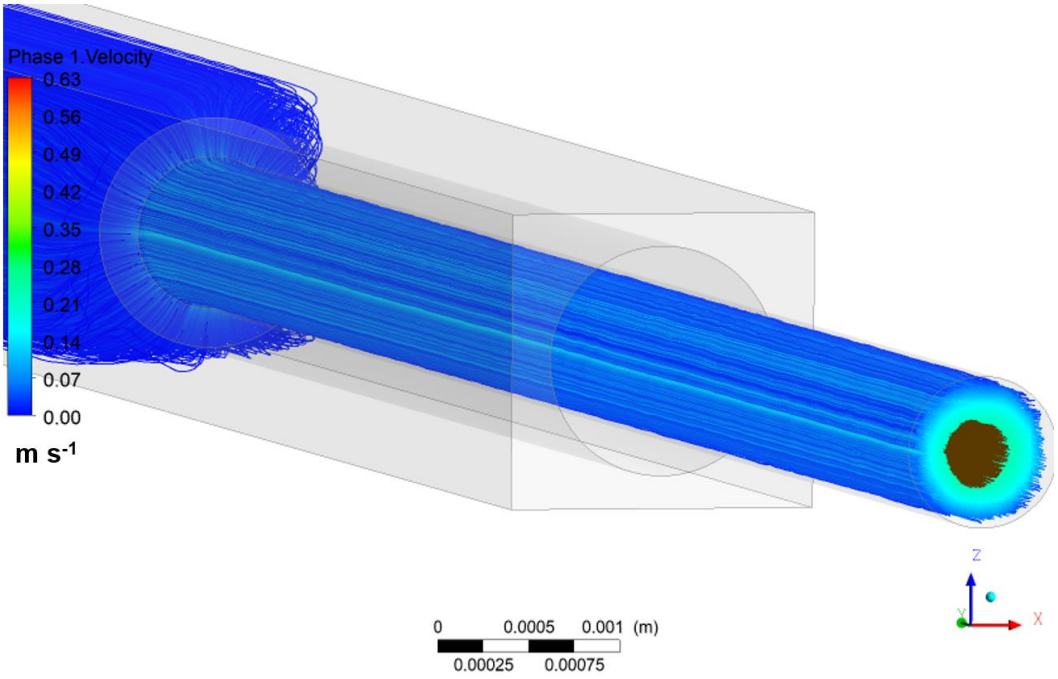

Fig. S4. CFD simulation showing the streamlines colored by velocity magnitude for CTAB solution (phase 1) (inlet flow rate of 3 mL min^{-1}) and the GO dispersion (inlet flow rate of 1.5 mL min^{-1} brown) inside of the main channel of the 3D hydrodynamic flow-focusing microfluidic device. 3D simulation of the flow behavior, coaxial flow of the CTAB solution around the GO fluid, originating the GO microfiber inside the device.

The electronic supplementary information video (SIV) represents the GO microfiber manufacturing process in the microfluidic device operating under the 3D hydrodynamic focusing principle. In the SIV video, the CTAB sheath flow was defined by the streamlines colored by the velocity magnitude and the GO microfiber in brown. The video shows a front view at the exit of the microdevice. It is possible to observe the brown GO microfiber in the center and, around it, the velocity streamlines of the CTAB coagulant solution. CTAB solution involves the GO microfiber in 360°, which is the main feature of 3D hydrodynamic focusing. The video was made with an arrow-line spacing factor of 0.0005 and a symbol size of 0.2 video settings.

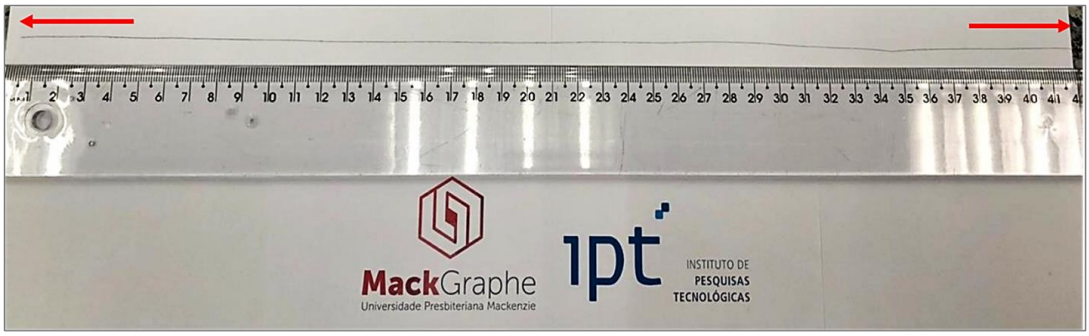

Fig. S5. Photograph of a GO microfiber obtained with the 3D flow-focusing microfluidic device.

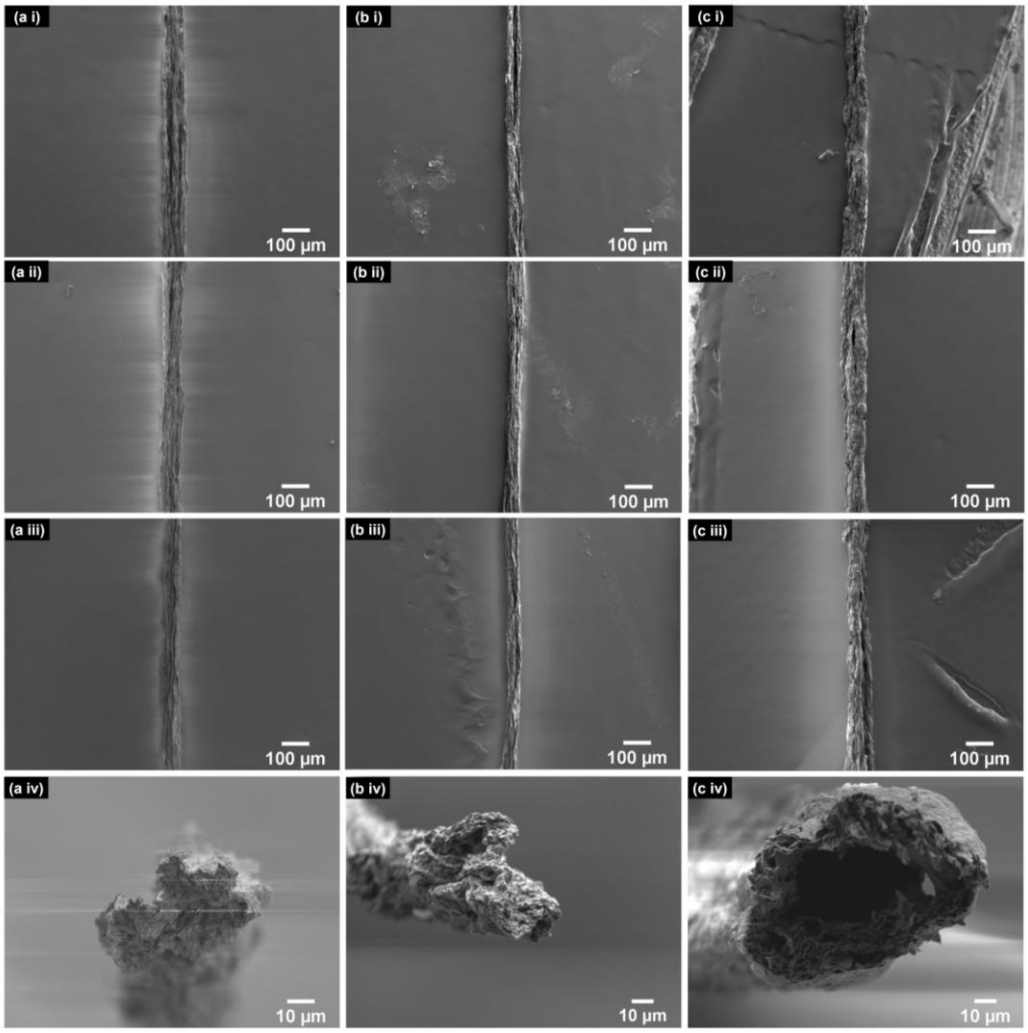

Fig. S6. Scanning electron microscopy (SEM) images at low magnification (100 x) of three different graphene derivatives microfibers: GO (a i-iii), rGO (b i-iii) and MW rGO (c i-iii). Cross-section image of GO (a iv), rGO (b iv) and MW rGO (c iv) microfiber.

Table S2. The diameter of the GO microfibers extract from the CFD simulation (Figure 2 (b)) for different values of flow rate (Q) ratio between the coagulant solution flow and GO dispersion flow. The diameters were extract using the Image J software.

Flow rate ratio $R = Q_{CTAB}/Q_{GO}$	Fiber diameter (μm)
2	349.44
4	237.43
6	213.91
7	206.07
8.7	183.69

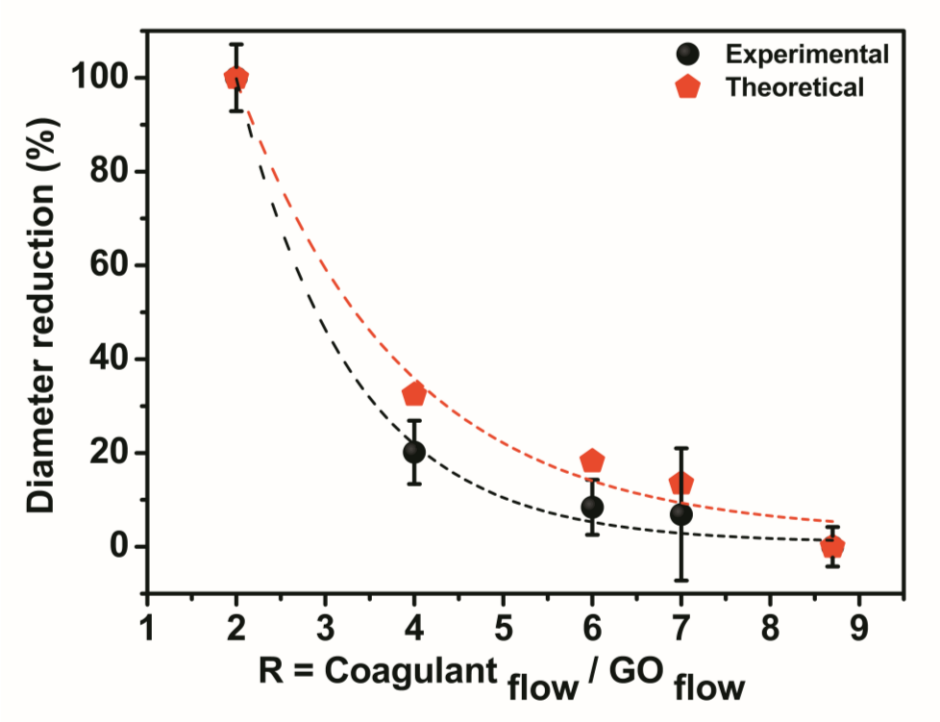

Fig. S7. Graphical showing the correlation between the experimental and theoretical diameter of the GO microfiber in the function of the flow rate ratio. $y = 467.1(\pm 92.8)e^{\left(-\frac{x}{1.3(\pm 0.2)}\right)} + 0.84(\pm 2.19)$ $R^2 = 0.993$ and $y = 282.0\ (\pm 69.3)e^{\left(-\frac{x}{1.9(\pm 0.5)}\right)} + 2.70(\pm 6.87)$ $R^2 = 0.976$, fitting equations for the experimental and theoretical results, respectively.

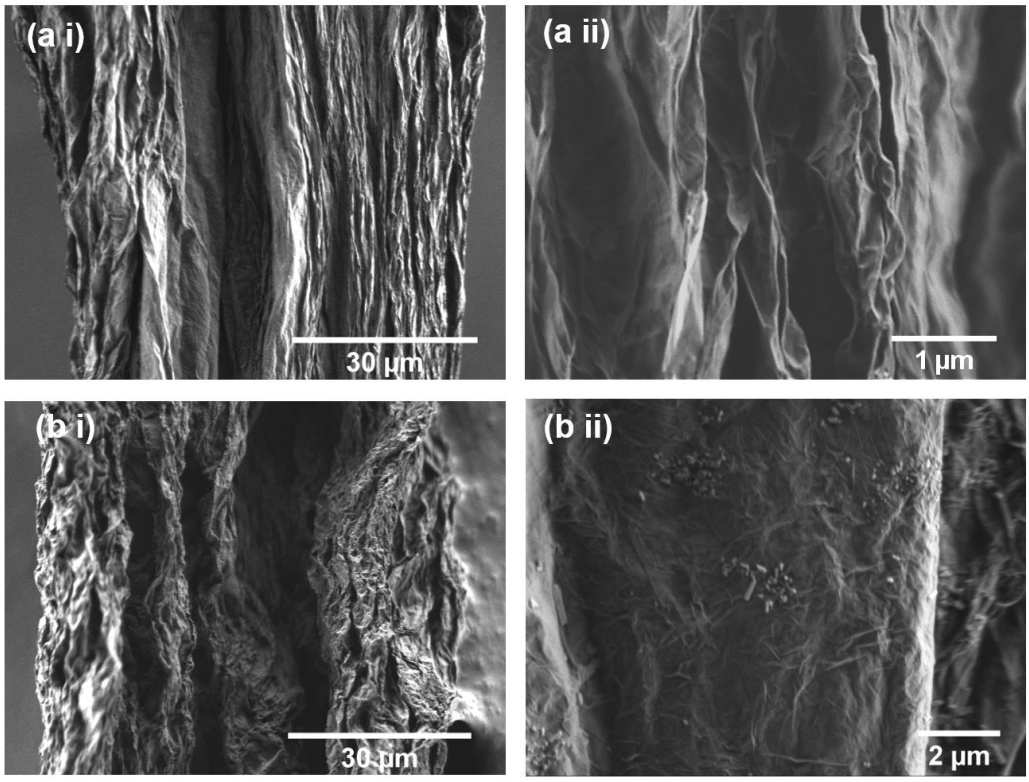

Fig. S8. SEM images of surface morphology of the GO (ai-ii) and rGO (bi-ii) microfiber.

Raman Spectroscopy – Calculation of the Crystalline Domain Size

The size of the crystalline domains (La) of the, can be estimated from the Raman signals using Equation S3, that was previously reported by Cançado *et al.*[4]

Equation S3 $$L_a(nm) = (2.4\ x\ 10^{-10}) \times \lambda^4 \times \left(\frac{I_D}{I_G}\right)^{-1}$$

Where λ (in nm), I_D and I_G represent the wavelength of the Raman laser (532 nm in this case) and the intensity of the D and G band, respectively.

The calculation of La was performed only for the MWrGO microfibers since for carbonaceous materials with I_D/I_G higher than 0.5 the equation S3 cannot be applied.

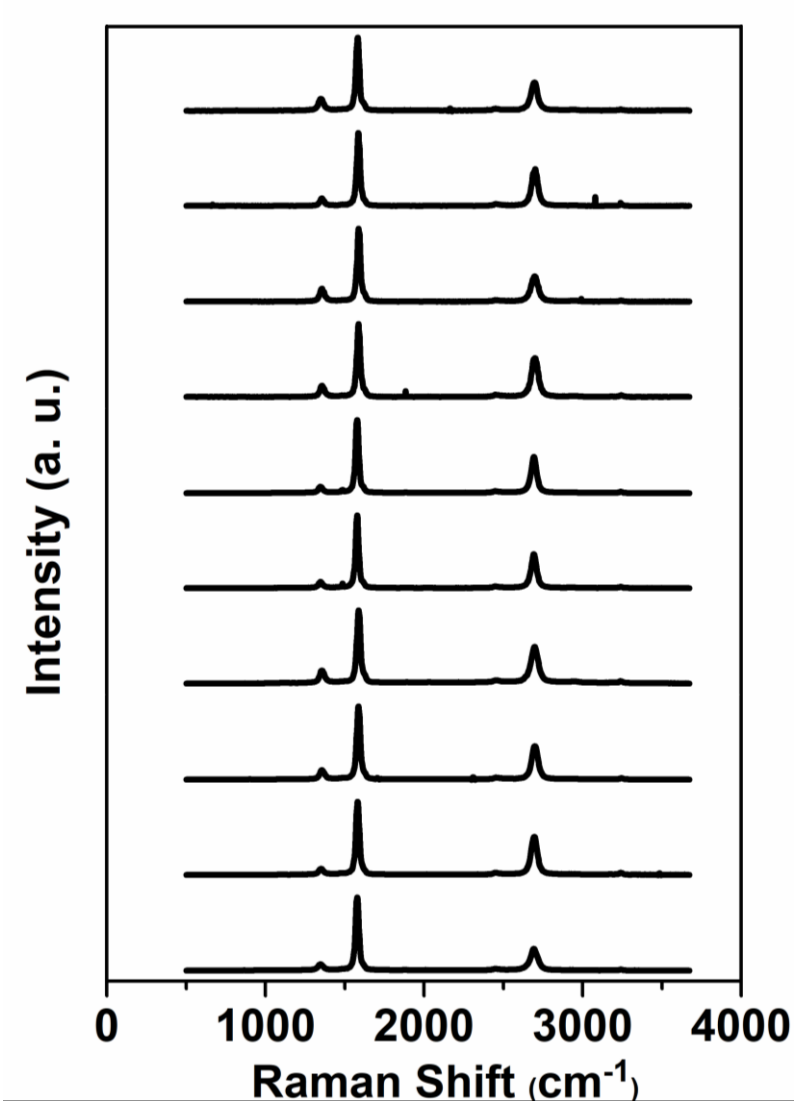

Fig. S9. Raman spectra for ten different MW rGO microfibers obtained in the same conditions.

Fourier-Transform Infrared Spectroscopy

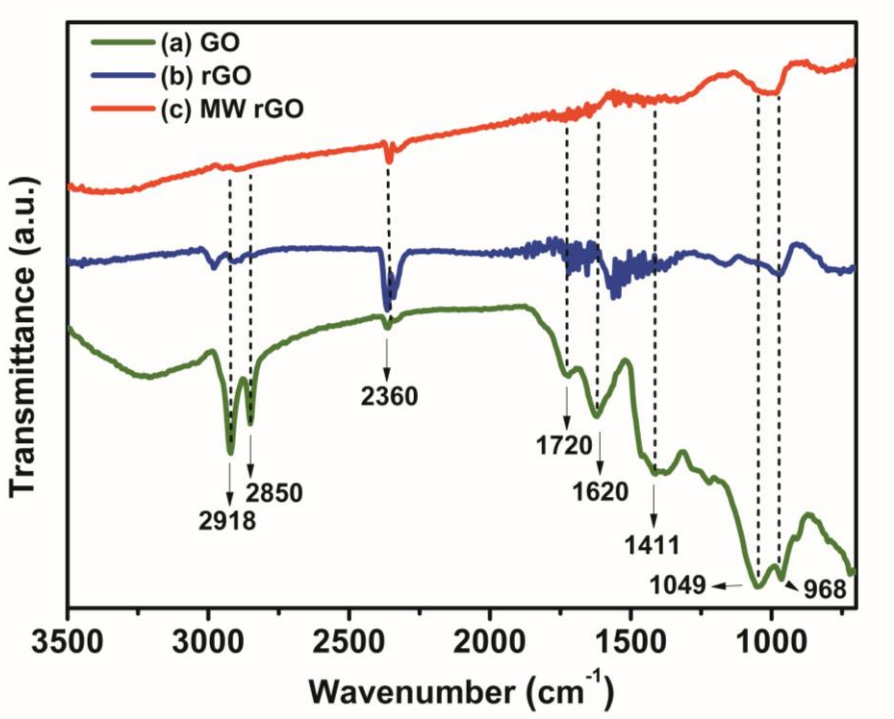

Fig S10. FTIR spectra from GO (a), rGO (b) and MW rGO (c) microfibers.

Figure S10 shows the FTIR spectra obtained for the GO (a), rGO (b) and MW rGO (c) microfibers. It is possible to see in the FTIR spectrum of the GO microfiber (Figure S10 (a)) two sharp peaks at 2918 and 2850 cm^{-1} related to the C-H stretching vibration modes of methyl and methylene groups from the presence of the CTAB[5,6] residues in the GO microfibers. After the thermal treatment (annealing at 300 ^{o}C at Ar/H_2 atmosphere) the intensity of these two peaks decreased (Figure S10 (b)) and totally disappeared after the MW treatment (Figure S10 (c)), proving that the microwave treatment degraded the CTAB residues. The FTIR spectrum for the GO microfiber (Figure S10 (a)) shows the typical features for the GO species. The bands at 1720, 1620 and 1411 cm^{-1} related to the vibrational modes of the carbonyl groups (C = O), alkenes groups (C = C) and hydroxyl groups (-OH) respectively[7,8,9,10]. The two peaks at 1049 and 968 cm^{-1} related to the epoxide groups[7,8,9,10]. Besides that, the band at 2360 cm^{-1} is related to the presence of $CO_2(g)$, possibly atmospheric[10]. After the reduction steps, the intensity of all the bands related to the oxygen functional groups decreased significantly due to the decrease of carbonyl, epoxides and hydroxyl groups in the structure of rGO and MW rGO microfibers, showing the effectiveness of the thermal and MW treatment.

Electrical Characterization in Air

For the determination of the electrical resistivity (ρ) of the graphene derivatives microfibers, the microfibers were deposited into glass slides and using a shadow mask (made by laser cutting in polyimide) and silver metal contacts were deposited along the x-axis of the microfibers, with the distance of 1 mm by 1 mm, using a silver ink (Neyco).

The distance between each electrode and the diameter of each evaluated microfiber was determined with an optical microscope (Olympus BX51M) and with the support of the Image J software.

First, the contact resistance (R_C) was obtained using the transfer length measurement (TLM)[11], where electrical resistance is measure as a function of distance defined by equation 4:

Equation S4:

$$R = \rho \frac{L}{A} + 2Rc$$

R is the resistance, ρ is the resistivity, A is the cross-sectional area of the fiber, L is the length between the electrodes and R_C the contact resistance.

The electrical measurements were done five times on each microfiber using a two-probe multimeter along the fibers.

Figure S8 shows the resistance vs. length plot for a typical rGO (a) and MWrGO (b) microfibers.

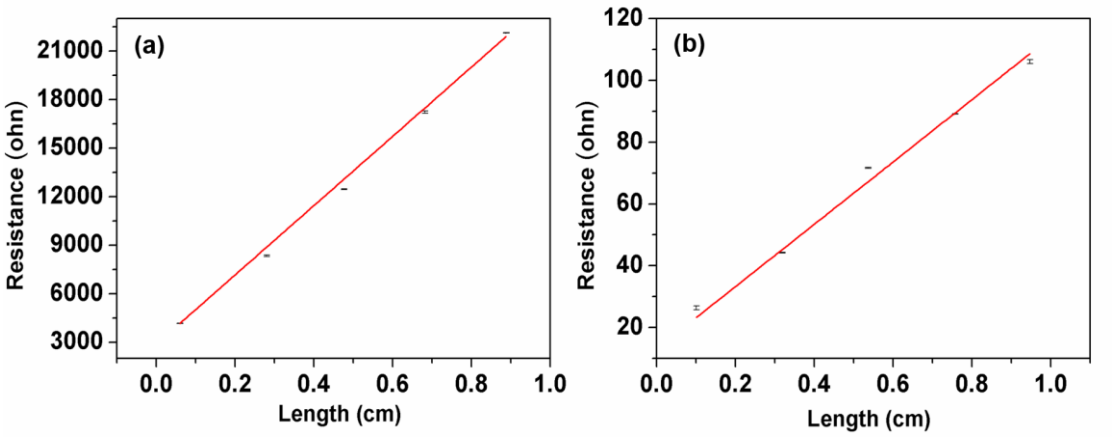

Fig S11. Resistance vs. length plot (n = 5) for a typical rGO, y = 2885.18 ± (60.70) + 21418,13 ± (361.79) x with R^2 = 0.99886 (a) and MWrGO, y = 13.10 ± (2.95) + 100.92 ± (4.67) x with R^2 = 0.99148 (b) microfibers.

The linear fittings of values in Figure S8 allows the calculation of the $R_{C,}$ which is the intercept of the linear fitting, which are 2.86 (±0.06) kΩ and 13.10 (±2.95) Ω for rGO and MWrGO microfibers respectively and the ρ that are 0.23 Ω.cm and 4.15x 10^{-3}Ω.cm for rGO and MWrGO microfibers respectively, after the extraction of the R_C contribution. This procedure was performed for 4 to 5 different rGO and MWrGO microfibers to calculate their conductivity, which is the inverse of the resistivity.

It was performed electrical resistance measurements in MW rGO microfibers with 5 cm of length, aiming to determine the conductivity of the MW rGO microfibers with higher length, using the configuration shown in the **Fig. S12.** For the MW rGO microfibers with 5 cm of length, the average conductivity is 1200.94 ± 219.34 S m^{-1}, a lower value than expected for the MW rGO microfibers with lower length, that may be related to non-uniformities in the microfibers and electron scattering effect along the x axis direction.

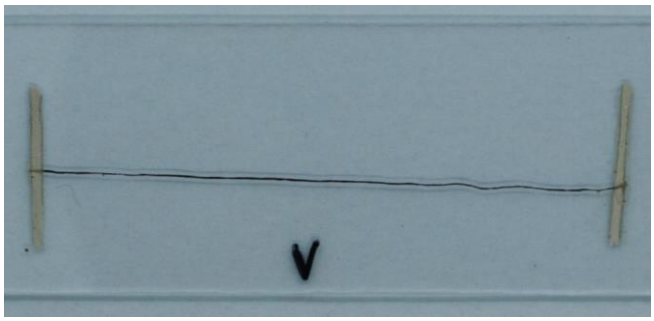

Fig. S12. Representative image of a MW rGO microfiber with 5 cm length contacted by silver electrodes used to perform the electrical characterization.

FET Based on Graphene Derivatives Microfibers Fabrication

The field-effect transistors (FETs) made of rGO and MW-rGO were fabricated in a two-terminal configuration using silver as contacts for both the source and the drain electrodes, deposited on top of a glass slide. A shadow mask was used for the correct deposition of the silver contacts. The metal contacts were passivated with a polydimethylsiloxane (PDMS) layer to guarantee that only the graphene derivatives microfibers were exposed to the electrolyte and avoid any faradaic process.

References

1 H. Cobas Gomez, R. Mansini Cardoso, J. de Novais Schianti, A. Marim de Oliveira and M. Gongora-Rubio, *Micromachines*, 2018, **9**, 285.

2 M. A. Santos, L. Marques and C. D. C. C. Silva, *Anal. Methods*, 2020, **12**, 3575–3581.

3 I. Ansys, *ANSYS Fluent Theory Guide. Release. ANSYS, Inc. Southpointe. 2600 ANSYS Drive. Canonsburg, PA 15317*, 2019.

4 L. G. Cançado, K. Takai, T. Enoki, M. Endo, Y. A. Kim, H. Mizusaki, A. Jorio, L. N. Coelho, R. Magalhães-Paniago and M. A. Pimenta, *Appl. Phys. Lett.*, 2006, **88**, 163106.

5 B. Baruah and M. Kiambuthi, *RSC Adv.*, 2014, **4**, 64860–64870.

6 G. Su, C. Yang and J.-J. Zhu, *Langmuir*, 2015, **31**, 817–823.

7 D. He, Z. Peng, W. Gong, Y. Luo, P. Zhao and L. Kong, *RSC Adv.*, 2015, **5**, 11966–11972.

8 G. Surekha, K. V. Krishnaiah, N. Ravi and R. Padma Suvarna, *J. Phys. Conf. Ser.*, , DOI:10.1088/1742-6596/1495/1/012012.

9 R. Al-Gaashani, A. Najjar, Y. Zakaria, S. Mansour and M. A. Atieh, *Ceram. Int.*, 2019, **45**, 14439–14448.

10 F. T. Johra and W.-G. Jung, *Appl. Surf. Sci.*, 2015, **357**, 1911–1914.

11 D. K. Schroder, *Semiconductor Material and Device Characterization*, John Wiley & Sons, Inc., Hoboken, NJ, USA, 2005.